J Nanostruct 16(4): 4664-4678, Autumn 2026

RESEARCH PAPER

Anti-Cancer Performance of Chitosan/Fe_3O_4 Nanohybrid for Magnetic Drug Delivery System

Ali Salah, Zaid H. Mahmoud *

Department of Chemistry, College of Sciences, University of Diyala, Iraq

ARTICLE INFO

Article History:
Received 12 April 2026
Accepted 15 July 2026
Published 01 October 2026

Keywords:
Biocompatible
Chitosan
Controlled drug release
Magnetic hyperthermia
Magnetite (Fe_3O_4) particles

ABSTRACT

This study aimed to prepare and evaluate chitosan hybrid nanoparticles with a magnetic inorganic component (Fe_3O_4) in different contents (C1-C4), as well as drug-loaded samples (D-C1 and D-C2). The goal was to assess the effect of component ratios on biocompatibility, active compound release, environmental response (pH and magnetic field), and thermal, structural, and magnetic properties. To achieve this, a range of instruments was used, including day 1 and day 5 photo-absorption measurements at concentrations of 50–200 µg/mL to assess cellular response, and cumulative drug-release studies over short time intervals (0–60 minutes). The analysis was prolonged (up to 350 hours) at pH 5.6 and 7.4, with or without a magnetic field (50 mT). Material characterization was performed using EDS, XRD, TGA/DTG, swelling measurements, magnetic (M–H) behavior, and thermal heating. The results showed that biocompatibility was best at lower concentrations (50 and 100 µg/mL), while absorption values gradually decreased at 150 and 200 µg/mL over time. Release was continuous and pH-dependent, with the highest rates in acidic environments, and the magnetic field accelerated release. This was consistent with EDS and XRD characterizations, which confirmed the incorporation of Fe_3O_4 into the chitosan matrix and an increased contribution of the inorganic phase with increasing Fe_3O_4 content. TGA/DTG analysis showed improved thermal stability as inorganic component content increased.

How to cite this article
Salah A., H. Mahmoud Z. Anti-Cancer Performance of Chitosan/Fe_3O_4 Nanohybrid for Magnetic Drug Delivery System . J Nanostruct, 2026; 16(4):4664-4678. DOI: 10.22052/JNS.2026.04.016

INTRODUCTION

Cancer treatment using nanotherapeutics, chemotherapy, and gene therapy has become a major research area in modern biomedical science [1]. Current drug delivery strategies primarily aim to increase the concentration of therapeutic agents at the tumor site while reducing their distribution to healthy tissues, thereby enhancing therapeutic efficacy and minimizing systemic toxicity [2,3]. Functionalized nanoparticles have attracted significant attention because they can protect drugs from premature metabolism and elimination, thereby improving pharmacological activity and reducing adverse effects [4]. Advances in nanotechnology have enabled the development of smart nanocarriers that selectively deliver therapeutic agents to cancerous tissues via receptor- and ligand-mediated targeting [5,6]. These nanocarriers can respond to external stimuli such as pH, temperature, enzymatic activity, magnetic fields, and ultrasound, thereby altering their physicochemical properties and

* *Corresponding Author Email: zaidhameed_91@yahoo.com*

enabling controlled drug release [7]. Among the various nanomaterials used in drug delivery systems, superparamagnetic Fe_3O_4 nanoparticles have shown considerable promise due to their multifunctional properties, including magnetic targeting, localized hyperthermia therapy, stem cell tracking, and magnetic resonance imaging applications [8,9]. The incorporation of Fe_3O_4 nanoparticles into polymeric nanocomposites enhances drug-delivery efficiency and enables magnetic guidance to tumor tissues [10-12]. Chitosan (CS) has emerged as one of the most promising biopolymers for biomedical and pharmaceutical applications because of its excellent biocompatibility, biodegradability, low toxicity, and ease of chemical modification [13]. Chitosan is a natural polycationic polymer derived from chitin and consists of 2-amino-2-deoxy-D-glucose and N-acetyl-2-amino-2-deoxy-D-glucose units linked by β(1→4) glycosidic bonds [14]. Due to the presence of amino and hydroxyl functional groups, chitosan exhibits strong interactions with drugs, proteins, and metal ions, making it highly suitable as a drug carrier [15]. In addition, chitosan possesses mucoadhesive and chelating properties that improve drug stability, enhance cellular uptake, and increase therapeutic efficiency [16]. Chitosan-based magnetic nanocomposites provide an effective platform for targeted drug delivery systems [17]. In these systems, Fe_3O_4 nanoparticles serve as magnetic carriers that can be directed to tumor tissues, while chitosan enhances nanoparticle stability, prevents aggregation, and controls drug release [18]. Furthermore, the pH-sensitivity of chitosan enables enhanced drug release in the acidic microenvironment of cancer tissues, thereby improving therapeutic outcomes and minimizing damage to healthy cells [19]. Doxorubicin (DOX) is one of the most widely used chemotherapeutic agents for cancer treatment because it interferes with DNA replication and inhibits topoisomerase II activity, leading to apoptosis and cancer cell death. However, conventional administration of DOX is associated with severe side effects and nonspecific toxicity. Therefore, loading DOX into chitosan-based magnetic nanocarriers has become an effective strategy to improve targeted delivery and reduce adverse effects [20]. In addition, multifunctional chitosan-based magnetic

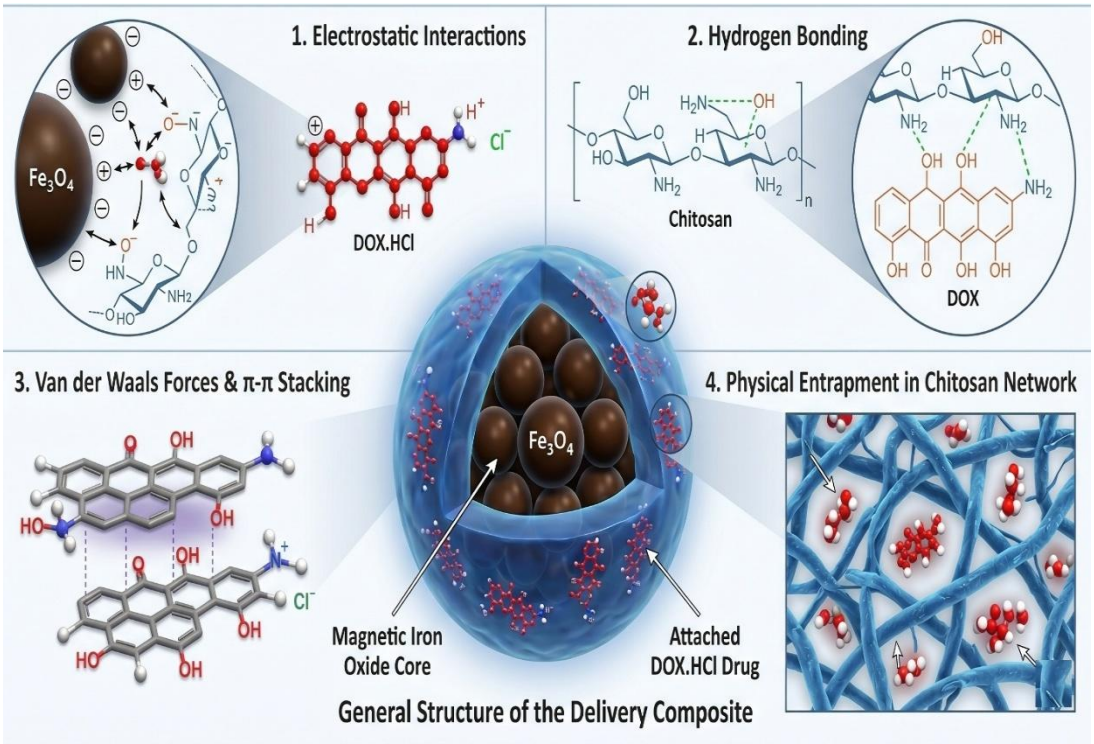

Fig. 1. Interaction ways between Fe_3O_4@CS with DOX drug.

nanocomposites have demonstrated high drug-loading capacity, controlled-release behavior, magnetic targeting capability, and enhanced anticancer activity [21]. Overall, chitosan-based magnetic nanocomposites represent a promising, biocompatible platform for cancer therapy due to their unique biological and physicochemical properties. These systems provide efficient drug loading, controlled release performance, selective tumor targeting, and reduced systemic toxicity, making them attractive candidates for advanced biomedical and therapeutic applications.

MATERIALS AND METHODS

Chemicals and reagents

Ferric chloride ($FeCl_3.6H_2O$, 99%), ferrous chloride ($FeCl_2.4H_2O$), sodium hydroxide (NaOH, 99%), and hydrochloric acid (HCl) were supplied from Merck Co. Chitosan (CS) (Mw. 190000 to 310000 Da) with a deacetylation degree of 80%, and Doxorubicin hydrochloride were purchased from Sigma Aldrich. The analytical-grade chemical materials were used as received, without further purification.

Preparation of Fe_3O_4

Fe_3O_4 NPs were prepared via the chemical co-precipitation method. Briefly, (5.41 g, 2 mmol) and (1.99 g, 1 mmol) of ferric and ferrous chlorides, respectively, were dissolved in 100 mL of deionized water under magnetic stirring. Then, 5 drops of ethylene glycol were added to the mixture as a surfactant material with continuous stirring. After that, 1 M of NH_4OH solution was added dropwise to the mixture until the pH reached 10. The black precipitate was separated by a magnet and washed several times with acetone and distilled water to remove the unreacted ions. Finally, the precipitate was dried for 4 h at 80 °C to obtain Fe_3O_4 [22].

Preparation of Fe_3O_4/chitosan nancomposite

Fe_3O_4/chitosan nanocomposites with different weight ratios were prepared via a solution-blending precipitation method. Briefly, 0.025 g of Fe_3O_4 NPs was dispersed in a 2.5 mL mixture of deionized water/ethanol and sonicated for 1 h. Separately, 0.075 g of chitosan was dissolved in 7.5 mL of 1% acetic acid under continuous stirring at room temperature for 12 h. After that, the Fe_3O_4 NP suspension was slowly added to the chitosan solution under continuous stirring for 5 h to ensure a homogeneous distribution. 1 M of NaOH was added dropwise with stirring until the pH reached 9, at which point a black-brown precipitate formed. The precipitate was isolated using an external magnet and washed several times with distilled water until the pH reached 7, then washed several times with ethanol to remove

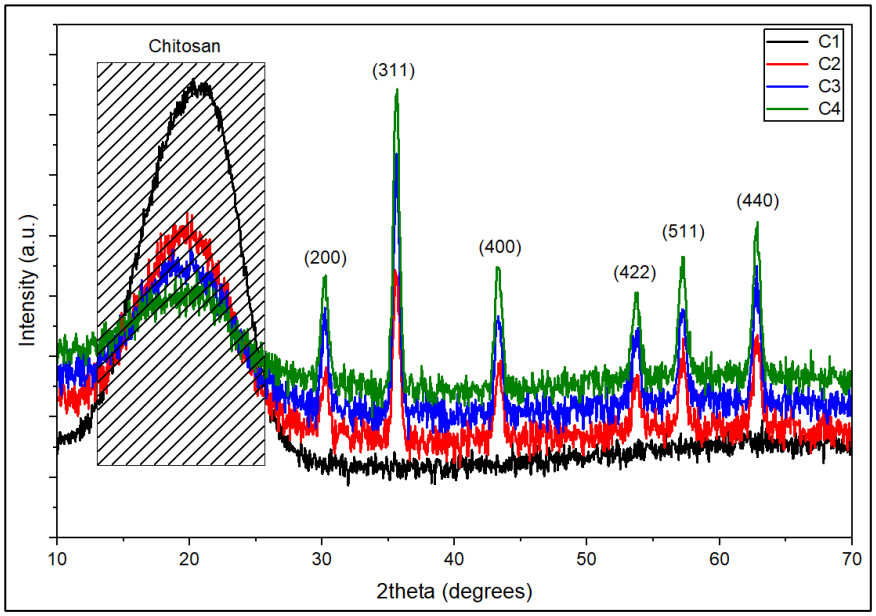

Fig. 2. XRD of bare and Fe_3O_4-incorporated chitosan.

residual acetic acid. Finally, the precipitate was dried at 60 °C for 6 h. The same producer was repeated using different ratios of chitosan (0.05 and 0.025 g) and Fe_3O_4 (0.05 and 0.075 g) [23].

Preparation of Fe_3O_4/Chitosan-Doxorubicin drug delivery system

100 mg of Chitosan(x)/Fe_3O_4(1-x) was dispersed in (5 mM, 20 mL) DOX solution under moderate sonication for 10 min to confirm uniform dispersion. Then, the mixture was stirred at room temperature for 6 h in the dark to permit enough reaction between the nanocomposite and the drug. Afterward, the Fe_3O_4/Chitosan-DOX was separated employing an external magnet, followed by washing with PBS to eliminate unbound DOX molecules. Finally, the prepared nanocomposite was dried at 30 °C for 6 h and stored in a dark container at 5 °C for further drug-release studies. The drug-loading capacity was investigated by monitoring the reduction in DOX concentration in the loading system following the incorporation of the prepared samples. The DOX Abs solution was examined at 480 nm before and after loading, and the concentration was calculated employing a standard calibration curve of Abs versus DOX concentration [24]. Possible interactions between Fe_3O_4@CS and DOX.HCl is exhibited in Fig. 1.

Cell viability examination

MTT assay

The MTT test is a colorimetric method used

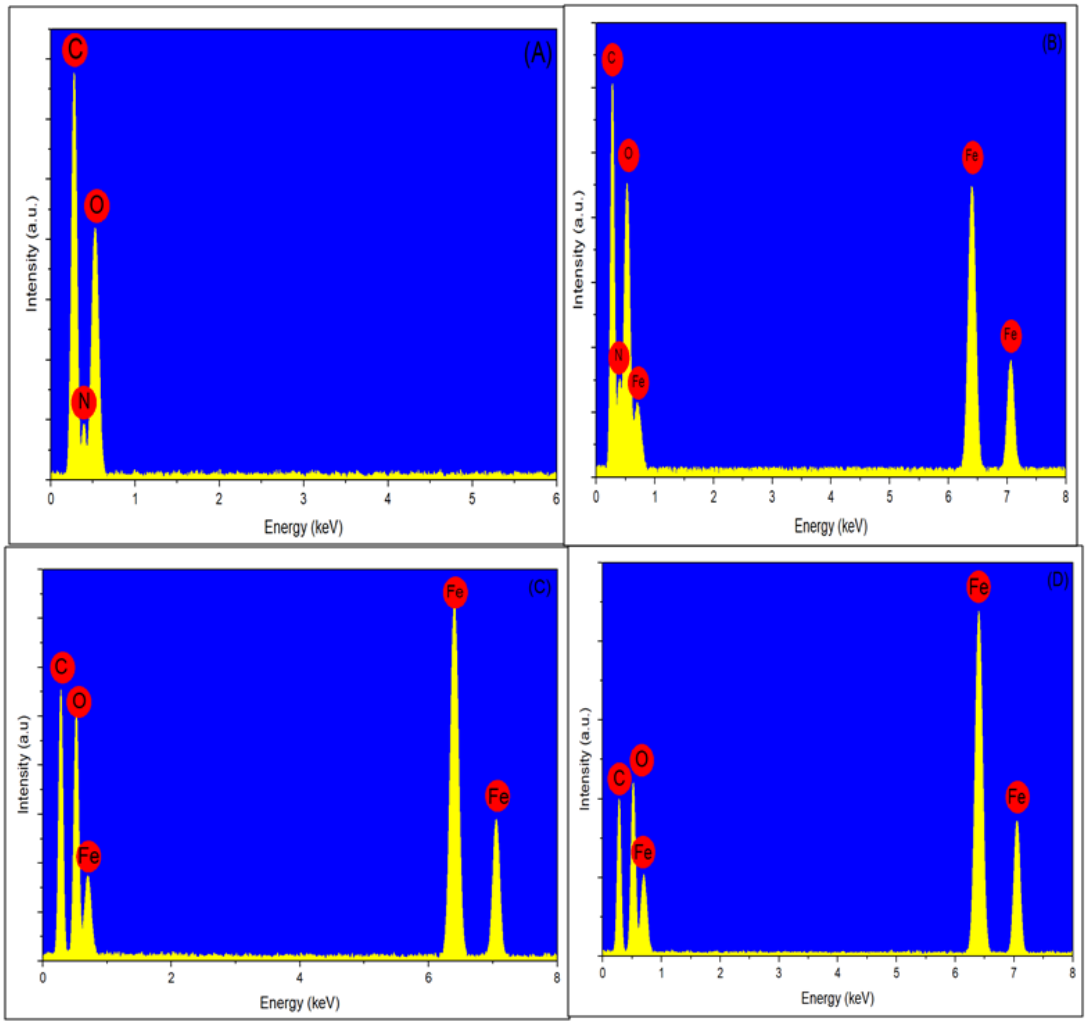

Fig. 3. EDX spectrum of (A) C1, (B) C2, (C) C3, (D) C4.

to assess cell viability, which depends on living cells' metabolic activity. This test is based on the reduction of tetrazolium dye to formazan crystals via mitochondrial dehydrogenases in living cells. After incubation, the crystals are dissolved employing DMSO, forming a colored solution. The color intensity, measured at 570 nm, is directly proportional to the number of metabolically active viable cells. HOS cells were cultured in 96-well dishes at a density of 5000 cells per well and maintained for 1 day to permit cell attachment. After incubation, the cells were cured with bare and (chitosan and cellulose)-incorporated Fe_3O_4 at different concentrations ranging from 20 to 100 µg/mL. Cell viability was assessed on the 1st and 7th days of incubation using the MTT assay. Then, 20 µL of MTT solution (5 mg/mL) was added to each dish, and the dishes were incubated for 2 h at 37 °C in 5% CO_2. Afterward, the formazan crystals were dissolved by adding 100 µL of DMSO to each dish, then maintained at 25 °C for 30 min to confirm solubilization before measuring absorbance at 570 nm. The same procedure was repeated on L929 cells, with cell viability estimated on the 1st and 7th days. In addition, the cytotoxic impact of the DOX-loaded bare and (chitosan and cellulose)-incorporated chitosan was investigated by treating cells with 10 µg/mL of each compound, followed by an MTT assay. Free DOX with a concentration of 58 µg/mL, equal to the DOX amount present in 10 µg/mL of DOX-Fe_3O_4/chitosan, was employed as the positive control.

Cytoskeleton staining

For cytoskeleton dying, HOS and L929 cells were cultured on surface-treated coverslips, placed in 12-well dishes at a density of 3000 cells/well, and maintained for 1 day to permit cell attachment. After the HOS and L929 cells gained an adherent morphology, they were treated with the prepared samples at a concentration of 10 µg/mL and incubated for 180 min. After incubation, the cells were washed with PBS and fixed with %4 PFA prepared in PBS for 30 min. Then, the cells were washed with PBS several times to remove excess fixative and permeabilized with 50% methanol. Afterward, the cells were blocked with 2% BSA for 30 min to decrease nonspecific binding. After removal of unbound BSA with PBS, the cells were stained with AF488 phalloidin prepared in 2% BSA for 1 h to visualize F-actin filaments. Finally, the nuclei were dyed with DAPI for 10 min. The dyed cells were washed with PBS and investigated under a fluorescence microscope at 358/461 nm.

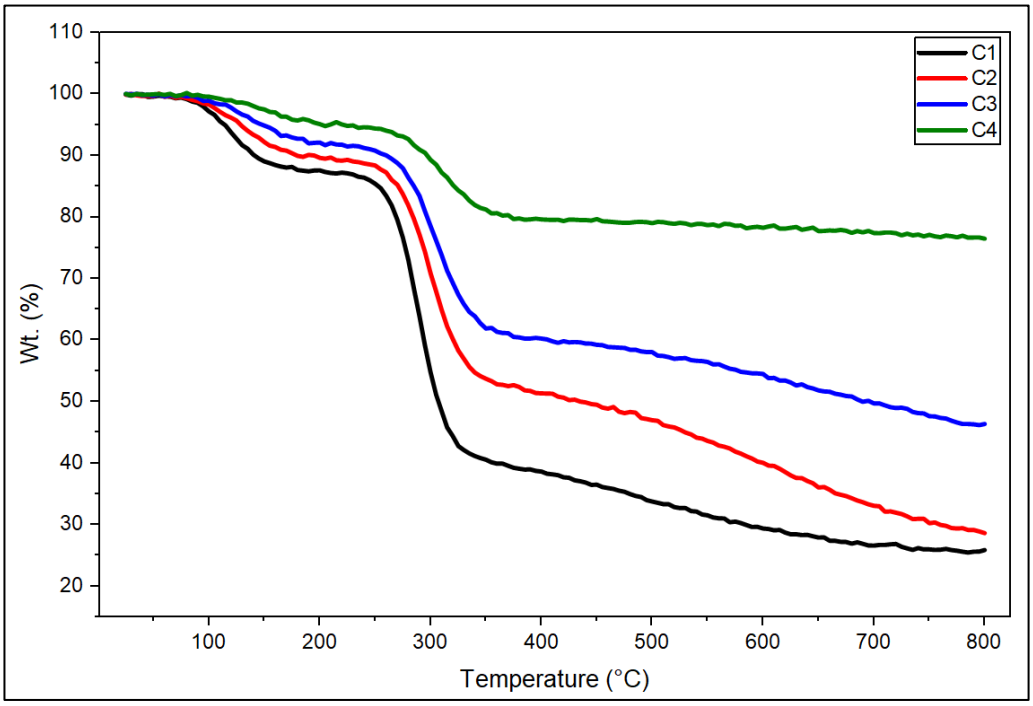

Fig. 4. TGA of C1-C4 compounds.

RESULTS AND DISCUSSION

XRD of bare and Fe_3O_4-incorporated chitosan is shown in Fig. 2. The results give clear proof of the successful introduction of Fe_3O_4 NPS into the chitosan matrix. For C1, which performs pure chitosan, a broad diffraction peak is observed at 20.27 °, indicating the semi-crystalline nature and is produced from the ordered configuration of chains kept via intra- and intermolecular H-bonding. The absence of sharp diffraction peaks in C1 suggests that chitosan is semi-crystalline rather than highly crystalline [25]. After the Fe_3O_4 incorporation in the C1 matrix, the XRD patterns of C2-C4 show several peaks centered at 2θ = 30.27 °, 35.45 °, 43.46 °, 53.75 °, 57.24 °, and 62.74 °, which correspond to (220), (311), (400), (422), (511), and (440) of spinel Fe_3O_4. The occurrence of these diffraction peaks suggests the existence of Fe_3O_4 NPs in the C1 structure. Among these diffraction peaks, the peak at 35.55 ° is the most intense and corresponds to the principal peak of Fe_3O_4, suggesting that magnetite retains its structure upon incorporation into the chitosan matrix. An imperceptible alteration in the diffraction is noted as the magnetite concentration increases from C2 to C4. In C2, the broad diffraction peak is still plainly visible, while the Fe_3O_4 diffraction peaks begin to show with mild intensity. This suggests that the polymeric C1 phase stays predominant, but Fe3O4 NPs have been incorporated into the C1 matrix. In C3, the distinctive Fe3O4 diffraction peaks become sharper and clearer, indicating a higher degree of crystallinity. In the C4 sample, the Fe_3O_4 diffraction peaks appear with the highest intensity, particularly at 35.59 °, 43.16 °, 57.18 °, and 62.74 °, suggesting that this structure includes the largest part of magnetite NPs. The reduction in the broad diffraction peak of chitosan after magnetite incorporation suggests that the crystalline Fe_3O_4 becomes the predominant phase contributor. In addition, the existence of a broad chitosan diffraction peak and the strong magnetite reflections emphasize the organic-inorganic formation, in which chitosan gives a semi-crystalline matrix while Fe_3O_4 keeps its spinel structure [26].

The EDX spectra of bare and Fe_3O_4-incorporated chitosan (C1-C4) are shown in Fig. 3 (a-d). The results emphasize the successful formation of chitosan-Fe_3O_4 at different ratios. The pure chitosan (C1) appears mainly with C and O signal peaks at 0.28 and 0.52 keV, respectively, which are assigned

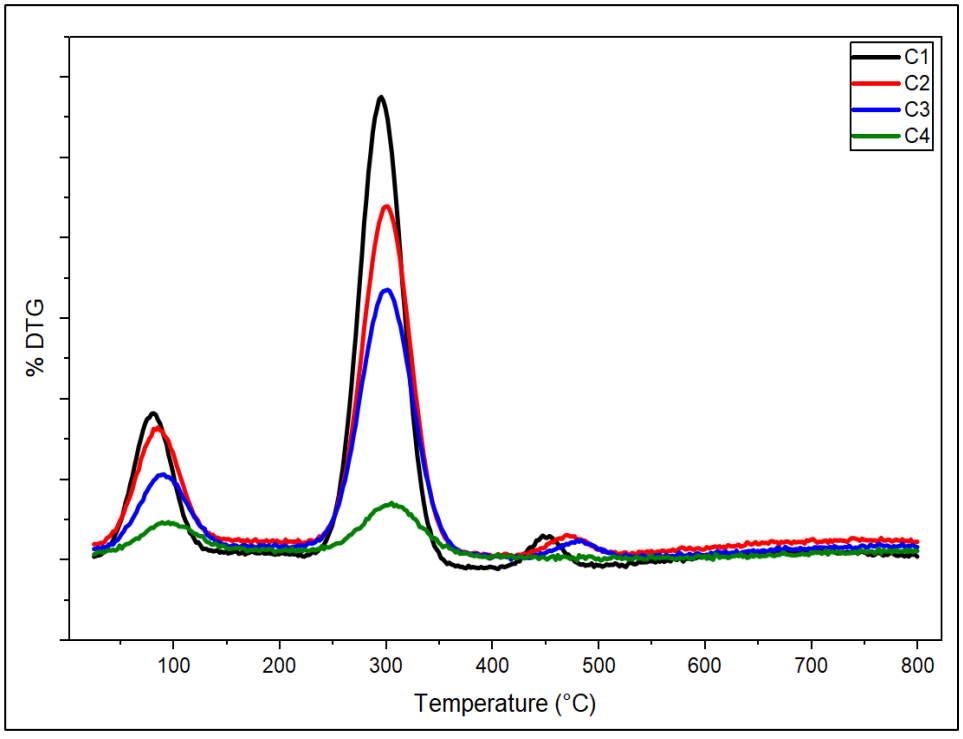

Fig. 5. DTG of C1-C4 compounds.

to the backbone containing C-OH, C-O, C-C, and glycosidic groups. Moreover, the results appeared to overlap with the N and O signals due to the low N content. After incorporating Fe_3O_4, the EDX spectra of C2-C4 show additional iron signal peaks, particularly at 6.4 and 7.0 keV, corresponding to the Ka and Kb signals, respectively, along with a Fe signal peak at 0.7 keV. The presence of these signals indicates the presence of Fe_3O_4 NPs within the chitosan polymer matrix. On the other hand, with increasing Fe content, the results appear to show an increase in Fe signal peak intensity, while reducing C and O signals from chitosan. This tendency suggests a progressive enrichment of the structure with the Fe_3O_4 phase. In addition, the results show no signal peaks from unexpected elements, indicating that the prepared compounds are comparatively pure, and that the EDX spectra are consistent with the XRD patterns.

The TGA curves of bare and %wt. Fe_3O_4-incorporated chitosan (C1-C4) is shown in Fig. 4. The results exhibited an enhancement in the thermal resistance of chitosan upon incorporation of Fe_3O_4. The C1 appears to show an initial slight weight loss below 120 °C due to the evaporation of adsorbed moisture, followed by a major thermal degradation step between 247 and 327 °C, which is assigned to depolymerization, deacetylation, and destruction of glycosidic bonds. Afterward, a gradual decrease is observed, reaching the lowest residue of about 25% at 800 °C. For the C2-C4 nanocomposite, the thermal degradation decreases with increasing Fe_3O_4 content. The main weight loss is attributed to chitosan backbone decomposition, but the curves are more gradual, and the final increase in residue is notable. This behavior suggests that magnetite acts as a thermal phase that limits the mobility of the chitosan chain, retards mass loss, and enhances the formation of higher inorganic residues. On the other hand, the interaction between NH_2 and -OH groups in Fe_3O_4 may enhance thermal stability by strengthening the chitosan network [27].

For bare and wt.% Fe_3O_4-incorporated chitosan, C1-C4: the results (Fig. 5) show a small peak at 100 °C, which is attributed to the evaporation of adsorbed H_2O. Moreover, the major peak is observed at around 195-315 °C and is assigned to chitosan backbone thermal decomposition, containing depolymerization, deacetylation, and

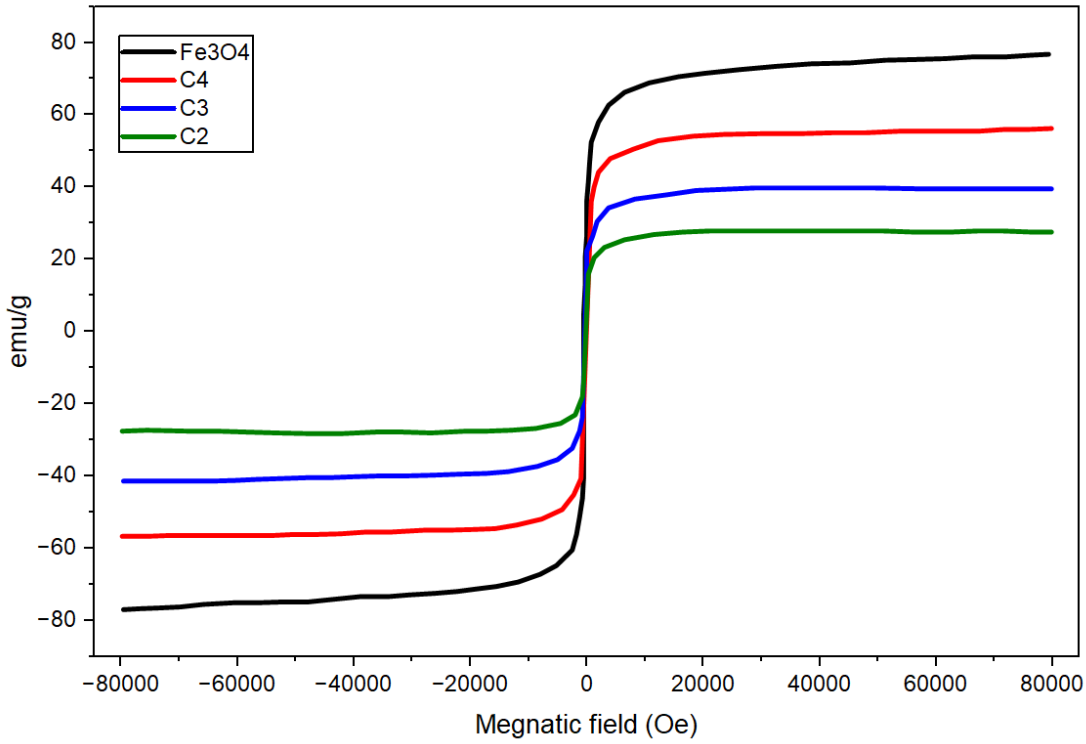

Fig. 6. VSM of bare and chitosan-incorporated Fe_3O_4.

glycosidic bond cleavage. The intensity of the major peak decreases with increasing magnetite content, indicating a lower organic mass-loss rate. C1 compound exhibits the sharpest and highest peak, with fast decomposition of the polymer. On the other side, C2-C4 compounds display lower decomposition peak intensities, indicating partial enhancement in thermal resistance because of the interaction between the $-NH_2$ and -OH function groups with Fe_3O_4 NPs. C4 shows the weakest thermal degradation peak, indicating the lowest thermal decomposition resistance among all prepared compounds. This demeanor is related to the higher magnetite content, which acts as a limited-chain-movement and thermally stable phase [28]. Generally, the DTG findings support the TGA results and emphasize that increasing magnetite content enhances the thermal stability.

The magnetic features of the prepared compound were investigated using VSM. The results appear to be a typical S-shaped magnetic demeanor for bare and (chitosan)/DOX-incorporated Fe_3O_4, as shown in Fig. 6. The Fe_3O_4 shows the highest saturation magnetization among all compounds, due to its inclusion of the largest fraction of the magnetic. After incorporation of chitosan and DOX, the MS gradually decreases due to the presence of organic materials surrounding the Fe_3O_4 NPs. This decrease doesn't indicate a lack of magnetic behavior, but it emphasizes the successful loading of chitosan and DOX onto Fe_3O_4 NPs. These organic materials can decrease the magnetic response by blocking magnetic interactions between Fe_3O_4 NPs and by increasing the non-magnetic fraction. The results exhibit small hysteresis and coercivity, suggesting that the prepared compounds behave as good magnetic materials, which is considered very important for medical drug delivery applications due to their ability to respond to an external magnetic field [29].

Cancer cell performance

The quantitative evaluation of proliferation and cellular viability was performed using the MTT assay to assess the biocompatibility of the prepared nanocomposites (C1-C4) in L929 and HOS cells. The MTT assay results indicate that the cytotoxic response of the prepared compounds was both time- and cell-type-dependent. The

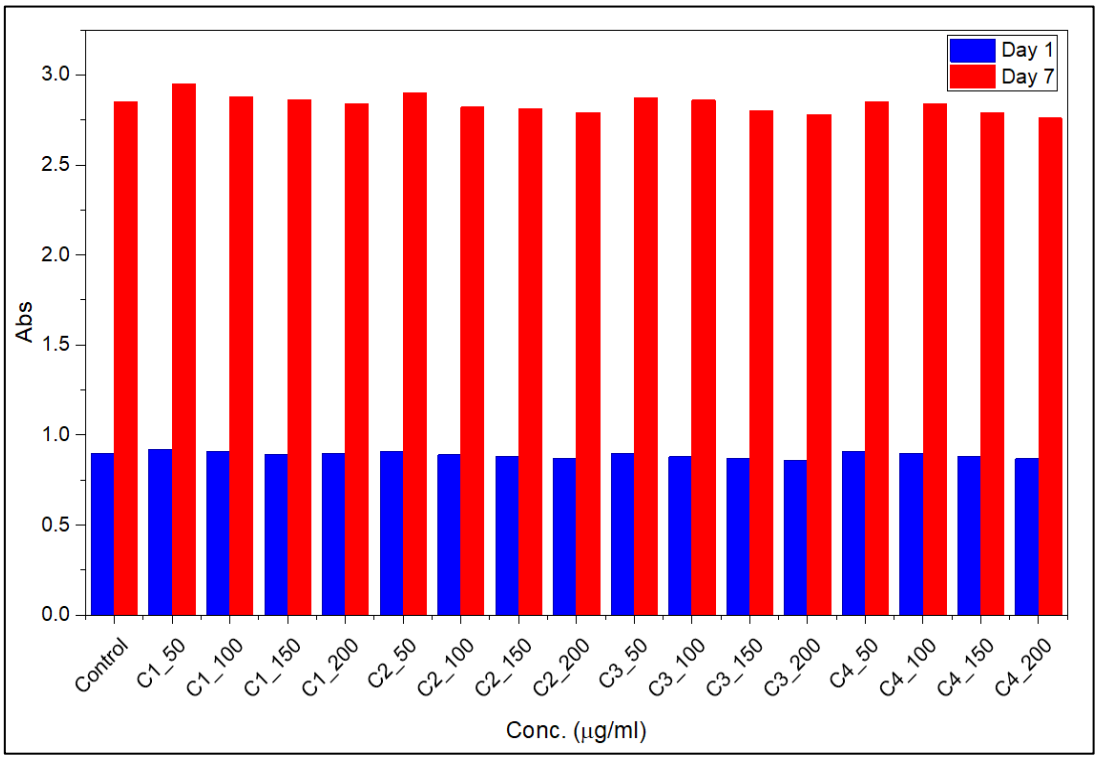

Fig. 7. Cell viability of control and C1-C4 compounds at different concentrations using L929 cells.

viability of the L929 cell stayed relatively high against all concentrations after 1 and 7 days, while the HOS appeared to decline more in cell viability, especially after long incubation for 7 days. These results indicate that the synthesized compounds exhibit selectivity, with lower toxicity to normal cells and greater inhibitory effects on cancer cells. In Fig. 7, the absorbance values measured on day 1 are similar to those of the control, indicating that none of the prepared compounds exhibited cytotoxicity at the studied concentrations. On the other hand, until after 7 days, the absorbance values remained high, with little fluctuation across different compounds and concentrations, indicating that the prepared compounds exhibit acceptable cytocompatibility with normal cells [30,31].

In contrast, the HOS cells appeared to have a notably different conductance (Fig. 8). On day 1, the Abs values were lower than those observed in L929 cells, indicating that HOS cells were more sensitive to the compounds at the early stage of exposure. This reduction becomes clearer on day 7, with a marked decrease in cell viability observed for most compounds, particularly at higher concentrations. The cumulative reduction in absorbance with boosting concentrations indicates a concentration-dependent antiproliferative effect, while the greater decrease after 7 days suggests a time-dependent response. So, the prepared compounds not only inhibit short-term metabolic activity but also interfere with long-term proliferation and HOS cells' survival. A comparison between the compounds suggests that their biological impacts aren't identical. Some prepared compounds showed higher viability in L929 cells while causing a greater decrease in HOS viability, indicating good selectivity between cancer and normal cells. This different response may be attributed to surface chemistry, composition, cellular uptake, particle-cell interactions, or the production of intracellular stress in cancer cells. HOS are more vulnerable to mitochondrial dysfunction, oxidative imbalance, and membrane disorders than L929 cells, which may explain why the cancer cells responded more strongly [32].

Fig. 9 shows the HOS cells' cytoskeletal morphology after therapy with the prepared compounds (C1-C4) at 50-200 mg/mL for 24h, where actin strings appear green, and nuclei

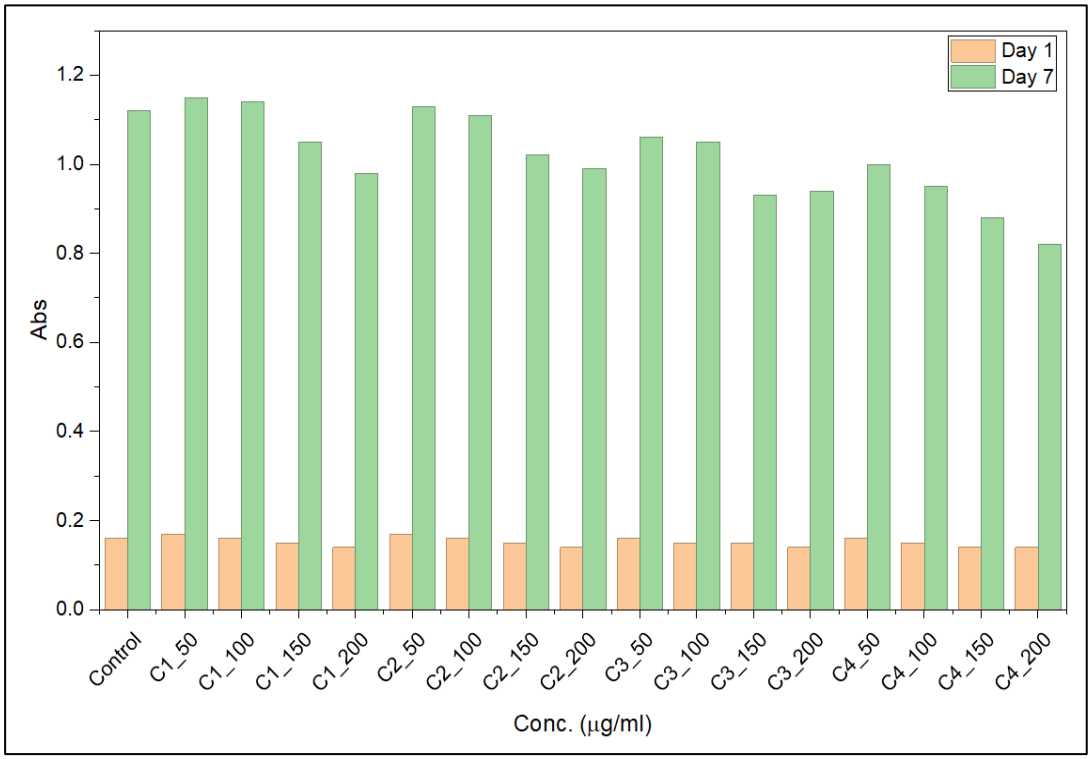

Fig. 8. Cell viability of control and C1-C4 compounds at different concentrations using HOS cells.

are shown blue with DAPI dye. The control cells appeared normal, with adhesive morphology, well-organized actin strings, uniformly stained nuclei, and extended spreading, suggesting the right cytoskeletal structure and normal cell attachment. Using bare and ferric oxide-doped chitosan, HOS cells remained detectable; however, clear alterations in actin organization and morphology were noted compared with the control. The actin network showed less regularity,

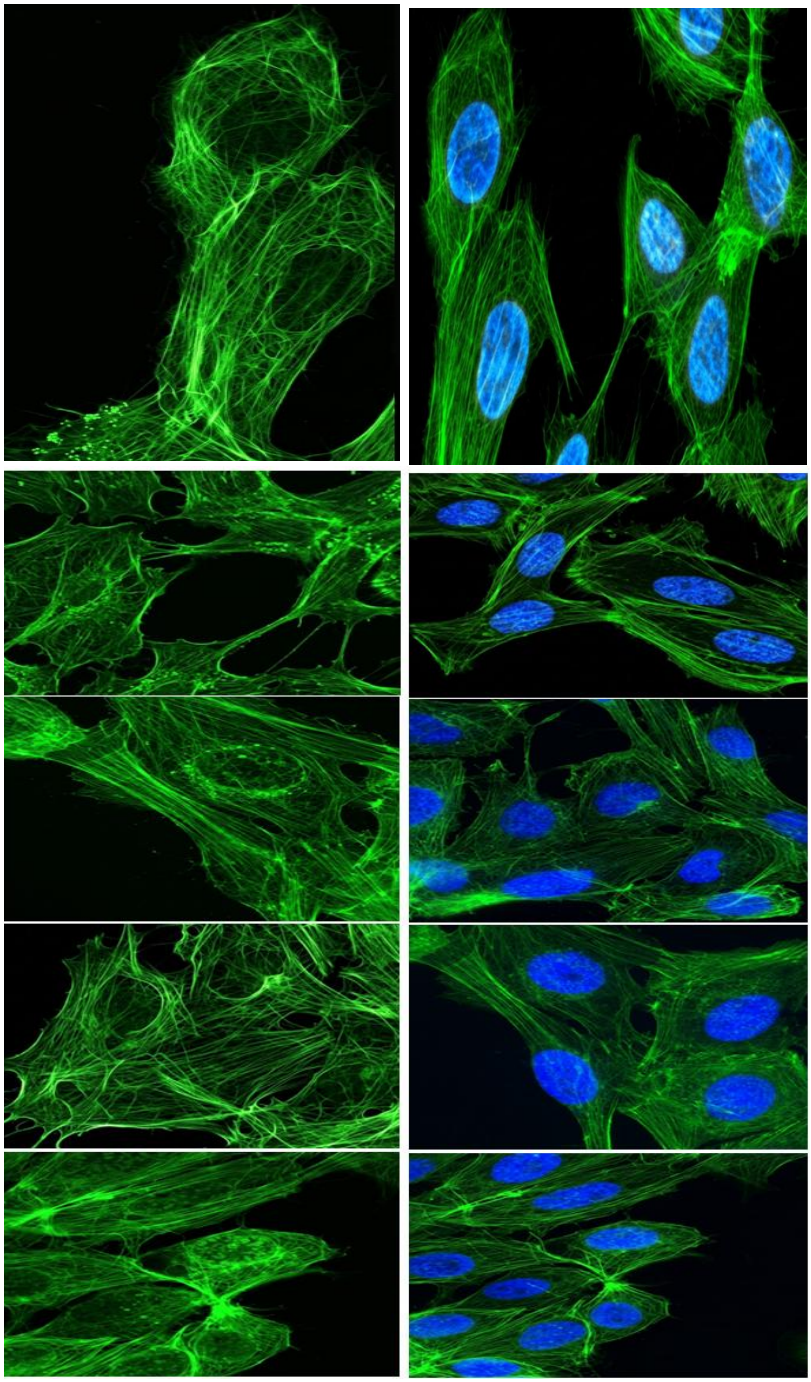

Fig. 9. cytoskeletal morphology after therapy with control (A,B) and the prepared compounds (C1-C4) (C-J), respectively.

and some cells appeared more contracted and less spread, suggesting cytoskeletal reorganization in response to therapy. Although the nuclei remained visible in all samples, the distribution of actin changed, indicating that the prepared compounds affected adhesion behavior and cellular architecture. The results suggest that the examined compounds induced mild structural changes in HOS cells without bringing immediate total cell death after 1 day. The noted alterations in actin string organization support the idea that the bare and ferric oxide-doped chitosan interfere with cytoskeletal integrity and may contribute to their anticancer activity and proliferative effects [33].

Fig. 10 displays confocal microscopy images of HOS cells attached to C1 and C2, with actin filaments shown in green and cell nuclei stained blue with DAPI. In both samples, the cells were fit to bind to the surface, ascertained by nuclear staining and clear actin. The combined images appear to be a successful cell-surface reaction. For chitosan, the cell appeared to have a comparatively good morphology, with organized actin organization and visible pervasion, suggesting favorable cohesion and preservation of cytoskeletal integrity. On the other side, the cells adhered to the C2 surface, but the actin array

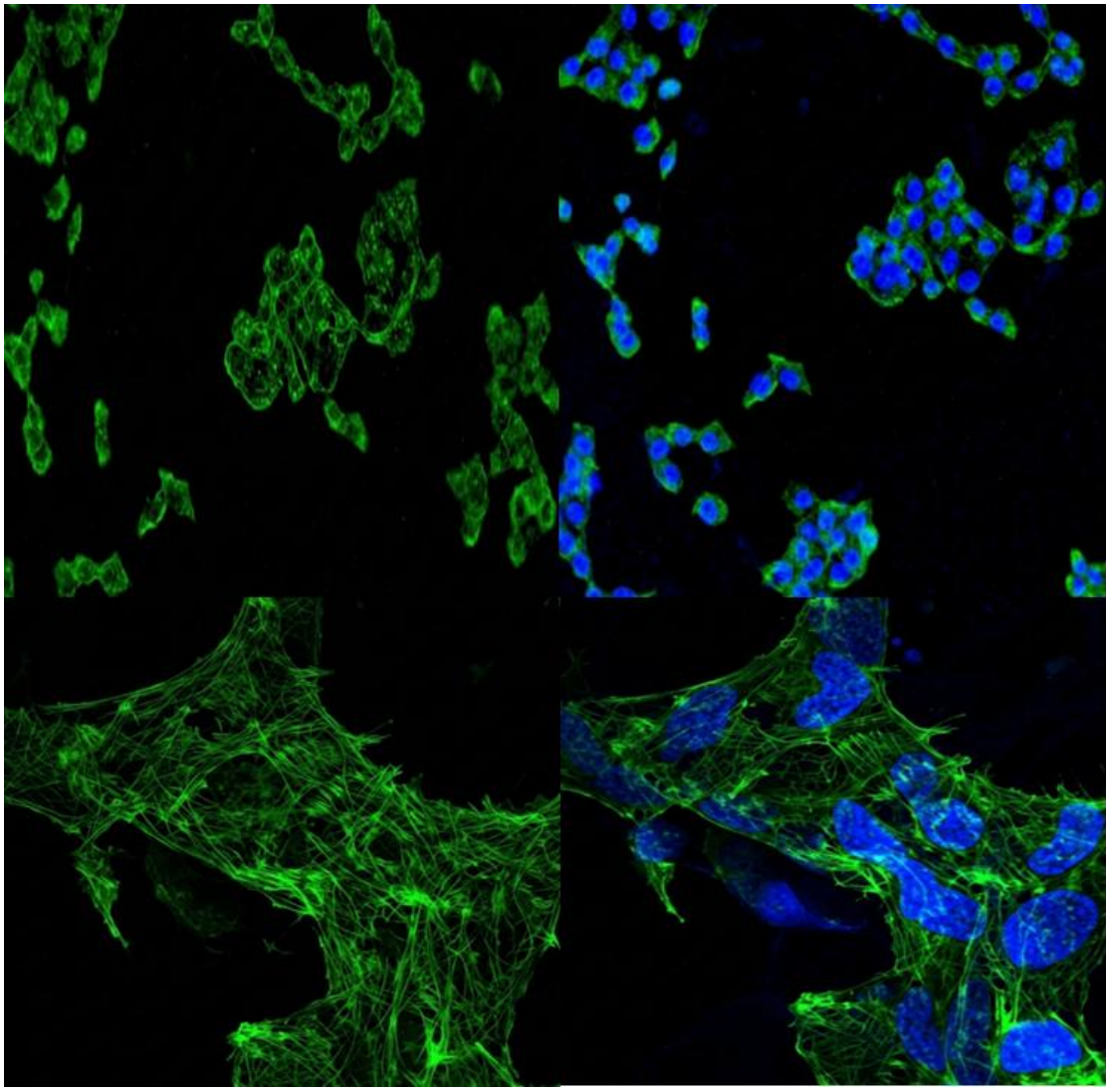

Fig. 10. Confocal morphology of HOS cells adhered to C1 and C2.

showed more clustered and irregular patterns in some regions, indicating a relatively altered cytoskeletal organization. Generally, the confocal images emphasize that both samples supported HOS cell cementation; however, the bare chitosan appeared to have better cytoskeletal organization and more regular cell morphology than C2. This indicates that surface composition affects cell cohesion behavior and structural organization [34].

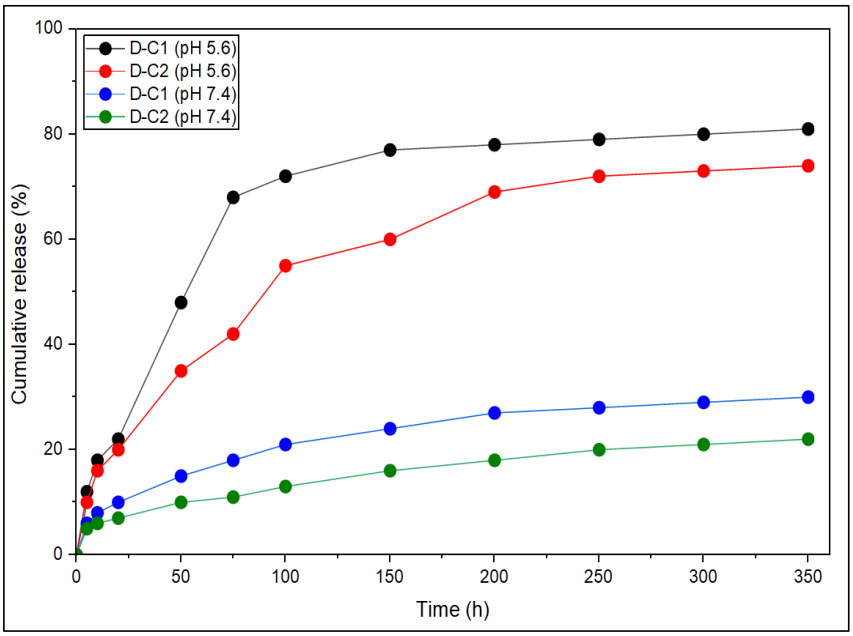

Fig. 11. DOX release profile of D-C1 and D-C2 at different pH.

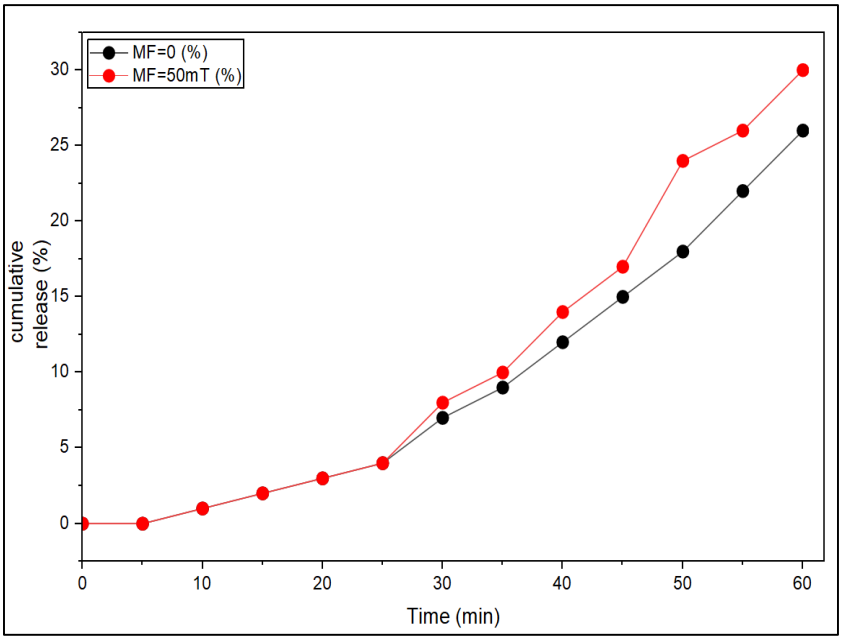

Fig. 12. DOX release profile of D-C2 at different mT and pH 5.6.

The DOX release curves of the C1 and C2 compounds at different pH levels and with a magnetic field are shown in Figs. 11 and 12. The results exhibit, at different pH levels (7.4 and 5.6), that the release of DOX from C1 and C2 is a burst at the initial 12h, which is due to the fast diffusion of DOX molecules on the surface of C1 and C2 compounds, followed by a decrease in release. At pH 7.4, C1 and C2 delivered 22% and 14% of DOX, respectively, over 100 h, and these ratios increased to 30% and 22% at 330 h. The Fe_3O_4 distributed in C2 also acts as a physical barrier, preventing matrix swelling and DOX transport, thereby reducing the diffusion rate. At pH 5.6, a consistent DOX release curve was obtained after 150h and 210 h for C1 and C2, respectively, suggesting that the DOX release had attained a steady state. In addition, the results show that C1 has a higher release rate than C2, due to its higher swelling index. The release rates at both pH values (7.4 and 5.6) invert the effect of swelling degree on the kinetics of DOX release from C1 and C2 porous compounds. Without a magnetic field (MF = 0), the DOX release is primarily diffusion-controlled, supported by matrix expansion due to pore-margin shifting and by the formation of cracks and breaks. Moreover, the lowest pH value improves the swelling index, thereby increasing the percentage of the DOX release [35].

The remote regulation of DOX release from D-C2 at pH 5.6 is illustrated with 50 mT, and the release results are shown in Fig. 12. The results showed that the DOX release percentage was considerably enhanced, 7% in 30 min and 31% in 60 min. The mechanism of magnetically induced DOX release can be attributed to the expansion and contraction of the chitosan network, resulting from differences in the orientation of Fe_3O_4 within it under a magnetic field. The relaxation and expansion of the Fe_3O_4/chitosan matrix enhance faster DOX release due to rapid diffusion. The remotely tunable DOX release can adjust the dosage, yielding a discrete therapeutic advantage over passive release [36].

The in vitro cell compatibility investigation of the DOX-incorporated (C1 and C2) is of eminent interest for locating their pharmacological efficacy. The study was carried out to assess drug release from C1 and C2 compounds using the MTT assay on L929 and HOS cells, as shown in Fig. 13A and 13B, respectively. In L929 and HOS cells, the viability index rose from 1 to 7 days for the control cells as a result of proliferation, while D-C1 and D-C2 showed a noted reduction in absorbance. In HOS cells, the results show a marked decrease in cell viability for D-C1 and D-C2 from 20 to 80 mg/mL, due to the higher percentage of DOX released at increasing concentrations. On day 1, both D-C1 and D-C2 exhibited similar cell-compatibility behavior, whereas on day 7, D-C1 showed greater apoptosis than D-C2 due to higher drug loading and release. In addition, the considerable decrease

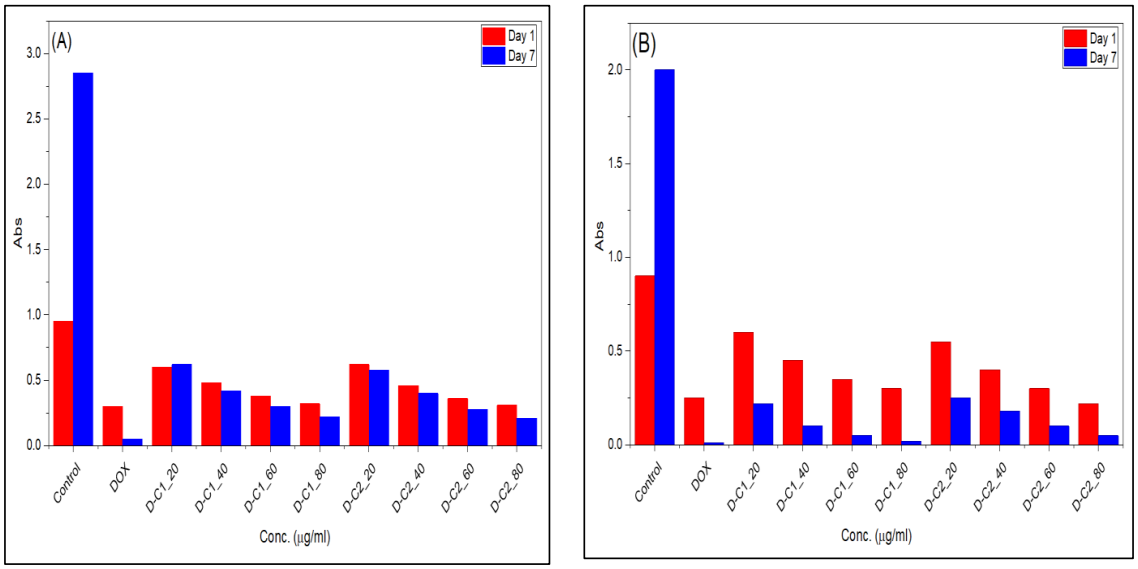

Fig. 13. MTT assay in (A) L929 and (B) HOS cells with DOX-C1 and DOX-C2 at different concentrations.

in Abs observed with free drug and DOX-(C1 and C2) inverts reduced cell population metabolic activity. It refers to DOX-induced toxicity, in which the released drug molecules damage DNA, causing to apoptosis. The free and DOX-loaded (C1 and C2) appear to induce DOX-induced toxicity in L929 cells; however, the cell damage is less pronounced than in HOS cells. Moreover, the results show a slight difference in cell viability between days 1 and 7 for D-C1 and D-C2.

CONCLUSION

The research demonstrated a tunable hybrid nanocomposite structure of chitosan and iron oxide particles that improves biocompatibility, drug release, and thermal and magnetic response, making it promising for targeted delivery and magneto-thermal therapy.

CONFLICT OF INTEREST

The authors declare that there is no conflict of interests regarding the publication of this manuscript.

REFERENCES

1. Li Q, Ma H, Zheng R, Cai L, Zhang Y, Ling Y, et al. Durvalumab Combined With Chemotherapy and SABR Therapy in Patients With Oligometastatic Non-small Cell Lung Cancer: A Multicenter Phase 2 Study. International Journal of Radiation Oncology*Biology*Physics. 2026;124(5):1371-1381.
2. Aundhia C, Parmar G, Talele C, Kumari M, Gupta G. Personalized Nanocomposite-based Drug Delivery Systems: Integration of AI and 3D Printing. Curr Drug Targets. 2026;27.
3. Haq Khan ZU, Khan TM, Khan A, Shah NS, Muhammad N, Tahir K, et al. Brief review: Applications of nanocomposite in electrochemical sensor and drugs delivery. Frontiers in Chemistry. 2023;11.
4. Sen A. Polymer nanocomposites in diabetes management: advances in biosensors and drug delivery systems. Discover Materials. 2025;5(1).
5. Saadat H, Aqsa A, Mujeeb ur R, Muhammad Raza S. Author response for "Targeted Drug Delivery: Designing Nanocarriers for Improved Therapeutic Action". Royal Society of Chemistry (RSC); 2026.
6. Zhu YF, He MQ, Lin CS, Ma WH, Ai Y, Wang J, et al. Multifunctional Nanocarrier Drug Delivery Systems: From Diverse Design to Precise Biomedical Applications. Advanced Healthcare Materials. 2025;15(2).
7. Molaveisi M, Zhao Y, Yu J, Shi Q. Lipid-based nanocarriers and their potential for incorporation into active edible films/coatings: highlighting nanocochleates as novel and promising nanocarriers. Critical Reviews in Food Science and Nutrition. 2025;66(7):1320-1363.
8. Azari E, Niad M, Nikmanesh H, Ahmadi AH. Fe_3O_4/SiO_2 core-shell nanoparticles: dual-targeting drug carrier for doxorubicin delivery in cancer therapy. Results in Chemistry. 2026;26:103181.
9. Sadr MS, Heydarinasab A, Panahi HA, Javan RS. Production and characterization of biocompatible nano-carrier based on Fe_3O_4 for magnetically hydroxychloroquine drug delivery. Polym Adv Technol. 2020;32(2):564-573.
10. Shirinova HA, Hajiyeva FV, Nuriyeva SG, Gahramanli LR, Karimova AH. The Governing Role of Polymer Matrix in Tailoring the Functional Properties of Magnetite-Filled Nanocomposites. Polymer Engineering & Science. 2026;66(5):3169-3179.
11. Hsu C-Y, Rheima AM, Kadhim MM, Ahmed NN, Mohammed SH, Abbas FH, et al. An overview of nanoparticles in drug delivery: Properties and applications. South African Journal of Chemical Engineering. 2023;46:233-270.
12. Mahmoud ZH, Al-Salman HNK, Hussein UA-R, Hameed SM, Hussein AA, Abbas JM, et al. Recent Advances in the Applications of Smart Nanomaterials in Biomedicine: A Review. Nano LIFE. 2025;16(03).
13. Kumar L, Aggarwal V, Rana R, Durgapal S, Verma H, Kushawaha SK, et al. The Nasal Route Redefined: The Impact of Chitosan Nanoparticles on Drug Delivery. Mini-Rev Med Chem. 2026;26(8):583-601.
14. Vashisth V, lakshmi, Dewangan HK, Sharma N, Jain D. Smart Delivery with Chitosan Nanoparticles: Current Innovations and Future Pathways. Drug Deliv Lett. 2026;16.
15. Jana S, Dewan D, Jana S, Sahu S, Jana P, Sahoo AK, et al. Green Nanotechnology: Chitosan Nanoparticles for Delivery of Medicinal Plant Extracts and Their Biomedical Impact. Drug Deliv Lett. 2026;16.
16. Ukwubile CA, Iliya I, Menkiti ND. Designing chitosan nanoparticles as a plant-derived drug carrier for brain tumor prevention and treatment. Advances in Traditional Medicine. 2026;26(2):449-464.
17. Lee YC, Kang IJ. Optimal Fabrication Conditions of Chitosan–Fe_3O_4–Gold Nanoshells as an Anticancer Drug Delivery Carriers. Bull Korean Chem Soc. 2017;38(3):313-319.
18. Characteristics and Magnetic Properties of Chitosan-Coated Fe_3O_4 Nanoparticles Prepared by Ex-Situ Co-Precipitation Method". Rasayan Journal of Chemistry. 2017.
19. Assa F, Jafarizadeh-Malmiri H, Ajamein H, Vaghari H, Anarjan N, Ahmadi O, et al. Chitosan magnetic nanoparticles for drug delivery systems. Crit Rev Biotechnol. 2016;37(4):492-509.
20. Li S, Xiao L, Deng H, Shi X, Cao Q. Remote controlled drug release from multi-functional Fe_3O_4/GO/Chitosan microspheres fabricated by an electrospray method. Colloids Surf B Biointerfaces. 2017;151:354-362.
21. Tuna Ş, Beyler-ÇIĞIl A, Demir S. "Preparation and Characterization of Hybrid Nanomaterials Containing Magnetic Fe_3O_4 Nanoparticles as Drug Delivery System ". Cellul Chem Technol. 2022;56(7-8):795-805.
22. Mustafa MA, Qasim QA, Mahdi AB, Izzat SE, Alnassar YS, Abood ES, et al. Supercapacitor Performance of Fe_3O_4 and Fe_3O_4@SiO_2-bis(aminopyridine)-Cu Hybrid Nanocomposite. International Journal of Electrochemical Science. 2022;17(10):221057.
23. Mahmoud ZH, Ajaj Y, Hussein AM, Al-Salman HNK, Mustafa MA, Kadhum EH, et al. $CdIn_2Se_4$@chitosan heterojunction nanocomposite with ultrahigh photocatalytic activity under sunlight driven photodegradation of organic pollutants. Int J Biol Macromol. 2024;267:131465.
24. Adimoolam MG, Amreddy N, Nalam MR, Sunkara MV. A simple approach to design chitosan functionalized Fe_3O_4

nanoparticles for pH responsive delivery of doxorubicin for cancer therapy. J Magn Magn Mater. 2018;448:199-207.
25. Meena HM, Kukreti S, Jassal PS. Fabrication of magnetic chitosan nanoparticles using iron oxide black, their characterization, and efficient adsorption of Zn (II), cd (II), Pb (II), and cu (II) ions from wastewater. Polyhedron. 2026;291:118080.
26. Philippou K, Christou CN, Socoliuc V, Vekas L, Tanasă E, Miclau M, et al. Superparamagnetic polyvinylpyrrolidone/chitosan/Fe_3O_4 electrospun nanofibers as effective U(VI) adsorbents. J Appl Polym Sci. 2020;138(15).
27. Wang Y, Li B, Zhen Y, Wang Y, Liu S, Chai Z. Removal of Congo red by core – shell magnetic chitosan submicrospheres: characterization and adsorption studies. Journal of Environmental Science and Health, Part A. 2025;60(11):599-607.
28. Zhang L-y, Zhu X-j, Sun H-w, Chi G-r, Xu J-x, Sun Y-l. Control synthesis of magnetic Fe_3O_4–chitosan nanoparticles under UV irradiation in aqueous system. Current Applied Physics. 2010;10(3):828-833.
29. Assessment of the Functionalization of Chitosan/ Iron Oxide Nanoparticles. Biointerface Research in Applied Chemistry. 2023;13(6):582.
30. Rajaei H, Mofazzal Jahromi MA, Khoramabadi N, Mohammad Hassan Z. Immunoregulatory Properties of Arteether in Folic Acid-Chitosan-Fe_3O_4 Composite Nanoparticle in 4T1 Cell Line and Mice Bearing Breast Cancer. Immunoregulation. 2019:207-220.
31. Mohammed L, Ragab D, Lin S, Said S, Gomaa H, Mequanint K. Preparation and Characterization of Glycol Chitosan-Fe_3O_4 Core–Shell Magnetic Nanoparticles for Controlled Delivery of Progesterone. Journal of Biomaterials and Tissue Engineering. 2017;7(7):561-570.
32. Mohamadi Bian E, Moghadam A. Synthesis and Characterization of Fe_3O_4 /Chitosan/TiO_2 Nanoparticle Novel Nanocarrier and Investigation of In Vitro Release of Vancomycin on HeLa Cancer Cell. International Journal of Biomaterials. 2025;2025(1).
33. Wang Y, Zhang L, Zhao G, Zhang Y, Zhan F, Chen Z, et al. Homologous targeting nanoparticles for enhanced PDT against osteosarcoma HOS cells and the related molecular mechanisms. Journal of Nanobiotechnology. 2022;20(1).
34. Guggenheim EJ, Khan A, Pike J, Chang L, Lynch I, Rappoport JZ. Comparison of Confocal and Super-Resolution Reflectance Imaging of Metal Oxide Nanoparticles. PLoS One. 2016;11(10):e0159980.
35. Unsoy G, Khodadust R, Yalcin S, Mutlu P, Gunduz U. Synthesis of Doxorubicin loaded magnetic chitosan nanoparticles for pH responsive targeted drug delivery. Eur J Pharm Sci. 2014;62:243-250.
36. Chen Z, Zhang P, Cheetham AG, Moon JH, Moxley JW, Lin Y-a, et al. Controlled release of free doxorubicin from peptide–drug conjugates by drug loading. Journal of Controlled Release. 2014;191:123-130.